PERGAMON

International Journal of Heat and Mass Transfer 44 (2001) 181–193

International Journal of HEAT and MASS TRANSFER

www.elsevier.com/locate/ijhmt

Transitional droplet growth and diffusion coefficients

P. Peeters*, C.C.M. Luijten, M.E.H. van Dongen

Department of Applied Physics, Eindhoven University of Technology, P.O. Box 513, 5600 MB Eindhoven, The Netherlands

Received 26 October 1999; received in revised form 4 February 2000

Abstract

The droplet growth models of Gyarmathy and Young, valid for arbitrary Knudsen numbers, are compared with experimental growth results obtained from expansion wave tube experiments. Growth experiments of *n*-pentanol in helium were performed at approximately 1 bar, resulting in growth curves stretching from the transition regime ($Kn \approx 1$) to the continuum regime ($Kn \ll 1$). Droplet growth experiments of water in helium and water in nitrogen were performed at elevated pressures, when the mean free path is small; hence, these growth curves are situated near the continuum regime. For $Kn > 0.1$, the Gyarmathy model appears to describe the experimental growth curves better than the Young model. However, for $Kn < 0.02$, the Young model gives the best results. For the water–helium and water–nitrogen systems new experimental diffusion coefficients are obtained, which are in good agreement with literature data.

1. Introduction

The growth of liquid droplets from a supersaturated vapour is a classical subject of interest in many fields of application. It is one of the key processes in aerosol science and cloud physics. It is important for condensate separation. On a more fundamental level, it is directly related to the investigations of nucleation, the formation of nuclei from which droplets grow. A review of theoretical droplet growth models is provided by Seinfeld and Pandis [1].

A very important parameter, when considering droplet growth, is the Knudsen number *Kn*. It is defined as the ratio of the mean free path of the molecules to the diameter of the droplets. For very large Knudsen numbers, the free molecular regime, growth is determined by the impingement rate of molecules onto the surface of the droplet. This was already described independently by Hertz and Knudsen [2,3]. In the limit of very small Knudsen numbers, the continuum regime, droplet growth in an inert carrier gas is controlled by diffusion. It is the transition zone between these two regimes ($Kn \approx 1$) which is of particular scientific interest. Several growth models describing droplet growth for all Knudsen numbers have been developed. Many of these models are based on the so-called flux matching method. Then, the system is divided into three regions, being a liquid phase and a continuum gas phase, separated by a Knudsen layer having a width of the order of the mean free path of the molecules. In this Knudsen layer gas kinetics apply, while continuum gas relations are applicable beyond this region. Assuming steady state conditions, mass and energy fluxes can be equated and thus obtained. This method was first applied by Fuchs [4] in 1934, who calculated only the mass fluxes. In 1970, Fukuta and Walter [5] extended the model to include the energy fluxes. The models considered here are those by Gyarmathy [6] and Young [7]. Gyarmathy modified a model based on the flux matching method, after comparing it with experimental results. What remained

* Corresponding author.

0017-9310/01/$ - see front matter
PII: S0017-9310(00)00098-3

Nomenclature

c	specific heat capacity
d	diameter
f_e	enhancement factor
h	specific enthalpy
k	thermal conductivity
m	molecular mass
n	number density
p	pressure
r	radius
t	time
y	mass fraction
D	diffusion coefficient
$\dot{E}$	total energy flux
Kn	Knudsen number
L	latent heat
M	total mass
$\dot{M}$	total mass flux
$\dot{Q}$	total heat flux
R	specific gas constant
S	saturation ratio
T	temperature
Z	compressibility

Greek symbols

α	coefficient
β	experimental coefficient
σ	surface tension
λ	mean free path
ρ	specific density

Subscripts

c	conduction
col	colliding molecule
con	condensation
d	droplet
ev	evaporation
g	gas
i	interface
id	ideal
l	liquid
m	at intermediate temperature
p	at constant pressure
s	gas phase at the droplet surface
tar	target molecule
v	vapour
0	initial
∞	at infinity

Superscripts

ct	continuum
fm	free molecular
m	molar
s	saturated

was an interpolating fit between the continuum and the free molecular regime.

The models will be compared with different sets of experimentally obtained growth curves, each set representing a different range of Knudsen numbers. Growth curves of *n*-pentanol in helium at atmospheric pressure and five different temperatures were previously obtained within the framework of an international collaboration on nucleation [8]. The curves stretch from the transition to the continuum growth regime. Furthermore, new experimental growth curves of water in helium and nitrogen have been obtained. These experiments were performed at elevated pressures. Therefore, the growth curves refer to the (near) continuum regime. It will be demonstrated that the validity of the growth models in this regime can be checked by using the diffusion coefficient as a free parameter.

2. Experiment

The growth curves are obtained using a pulse expansion wave tube. This device can be used to study nucleation as well as droplet growth, and has previously been described in Refs. [9–11]. Peters and Paikert used a similar device [12], allowing them to measure both the growth and subsequent evaporation curves of the droplets [13]. The set-up, as it was used

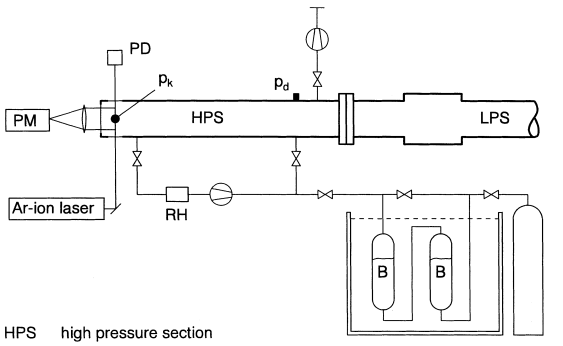

Fig. 1. Schematic view of the experimental set-up.

here, is schematically shown in Fig. 1. The high pressure section (HPS) is filled with the gas–vapour mixture under study, via a saturating bubbler set-up. The vapour fraction can be varied by changing the amounts of dry and saturated carrier gas let in. Homogeneity is established by the mixing pump in the mixing circuit. The final vapour fraction is determined by means of a specially calibrated Vaisala humidity sensor, type HMP 234 [14]. When the diaphragm between the HPS and LPS is ruptured, a homogeneous monodispersed cloud of droplets is formed at the end wall of the tube due to a short duration pulse in the supersaturation. After this pulse, the gas–vapour mixture is still in a supersaturated state, allowing the formed droplets to grow. Since the nucleation (droplet formation) rate is extremely nonlinearly dependent on the supersaturation, no significant nucleation will occur after the pulse.

The pulse-shaped maximum in the supersaturation is directly related to the pressure signal, shown in Fig. 2. Also shown are a schematic view of the tube and the propagation of the subsequent pressure waves in time. When the diaphragm ruptures, a shock wave travels into the LPS and an expansion fan travels into the HPS. When the head of the expansion fan reflects at the end wall of the HPS, the pressure will start decreasing. After the reflection has been completed, the pressure at the end wall is constant again. In the meantime, the shock wave travelling into the LPS encounters a widening. As a consequence, a weak expansion fan followed by a small recompression wave is reflected into the HPS, travelling behind the strong expansion fan. This forms a small pressure dip at the beginning of the low pressure plateau. Since the whole process is adiabatic, the temperature signal will have a similar profile as the pressure signal. As pressure and temperature drop, the gas–vapour mixture will become supersaturated, with the saturation ratio S having a maximum value during the pressure and temperature dip.

Droplet size and density at the end wall of the HPS are determined by a combination of constant angle Mie scattering (CAMS) and light extinction, while the pressure history at the endwall of the HPS is determined by means of a Kistler 603 B piezoelectric pressure gauge.

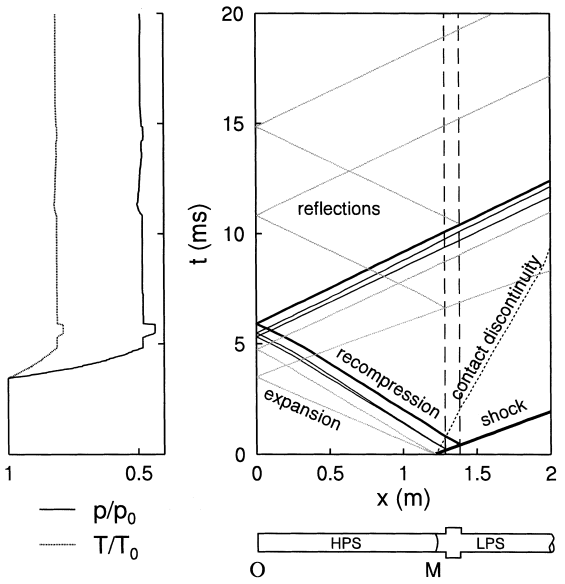

Fig. 2. Wave propagation in the expansion wave tube with the corresponding pressure and temperature signals at the end wall.

3. Theory

The theoretical description of droplet growth is based on the assumption of quasi-steadiness. The pressure is uniform, and the droplet is fixed in its environment. The droplet is assumed to be spherical and in thermodynamic equilibrium with its surface. In the cases studied here the vapour mass fraction is always small ($y_v \ll 1$).

3.1. The Young model

In the model by Young [7], the growing droplet is divided into three different regions, as is shown in Fig. 3. The first region is the droplet of radius r_d. It is assumed to be in equilibrium with its surface and to have a uniform temperature T_d. The second region is the so-called Knudsen layer. It directly surrounds the droplet and has a width of the order of the mean free path of the molecules. The third region, beyond the Knudsen layer, is the continuum region. The Knudsen layer and the continuum region are separated by the fictitious interface i at a distance r_i of the centre of the droplet.

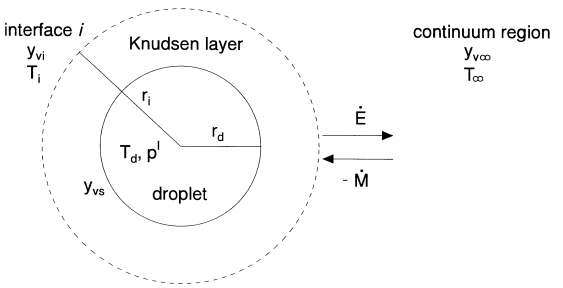

Fig. 3. Schematic view of a growing droplet.

In the continuum region mass and energy fluxes ($\dot{M}$, $\dot{E}$) are related to differences in temperature and vapour mass fractions (y_v) at the interface i and the far field. Using continuum gas relations the mass and energy fluxes can be calculated [7,10]. The results are (see Appendix B)

$$\dot{M} = 4\pi r_i \rho_m D_m (y_{vi} - y_{v\infty}), \tag{1}$$

$$\dot{E} = \frac{1}{2}\dot{M} c_{pv}(T_i + T_\infty) + 4\pi k_m r_i (T_i - T_\infty), \tag{2}$$

where ρ denotes the density and k the thermal conductivity of the gas–vapour mixture, D is the diffusion coefficient, and c_{pv} is the specific heat capacity of the vapour at constant pressure. The subscript m denotes that the quantities are evaluated at an intermediate temperature T_m. The right hand side of Eq. (2) contains two terms: the first term describes the energy transport directly resulting from mass transport, while the second term describes the energy transport due to conduction. Conservation of momentum yields that the pressure p is uniform throughout the system, whenever the Mach number of the condensing vapour is small.

In the Knudsen layer kinetic gas theory applies. All the molecules that leave the droplet surface are assumed to have a Maxwellian velocity distribution at temperature T_d. All molecules have fully thermally accommodated before they reflect or evaporate. Hence, although gas molecules do not condense, they do contribute to the total energy flux. At the interface i a Maxwellian velocity distribution is not appropriate, since there a non-equilibrium situation exists. Young [7] argues that the Grad velocity distribution [15,16] gives a physically realistic representation of the diffusive and convective mass and heat fluxes near the interface. Consequently, assuming that molecules travelling through the Knudsen layer do not collide, all the molecules coming towards the droplet have a Grad velocity distribution at temperature T_i. Using these velocity distributions and the appropriate conditions for incoming and outgoing molecules, the mass and energy fluxes in the Knudsen layer can be calculated, resulting in [7,10]

$$\left(1 - \alpha_{con}\frac{r_d^2}{2r_i^2}\right)\dot{M} = 4\pi r_d^2\left(\frac{\alpha_{ev}\rho_{vs}R_v T_d}{\sqrt{2\pi R_v T_d}} - \frac{\alpha_{con}\rho_{vi}R_v T_i}{\sqrt{2\pi R_v T_i}}\right), \tag{3}$$

$$\dot{E} = 4\pi r_d^2\left[\frac{\rho_{vi}R_v T_i\left(c_{pv} - \frac{R_v}{2}\right)}{\sqrt{2\pi R_v T_i}} + \frac{\rho_{gi}R_g T_i\left(c_{pg} - \frac{R_g}{2}\right)}{\sqrt{2\pi R_g T_i}}\right](T_d - T_i) + \frac{r_d^2}{2r_i^2}\dot{Q}_{ci} + \dot{M}c_{pv}T_d - \dot{M}\frac{R_v}{2}T_d\left(1 - \frac{r_d^2}{2r_i^2}\right) - \frac{r_d^2}{2r_i^2}\dot{M}c_{pv}(T_d - T_i). \tag{4}$$

R_v and R_g are the specific gas constants of the vapour and the gas, respectively, and α_{ev} and α_{con} denote the probability that an attempt to evaporate or condense is successful. We will take both probabilities equal to one, as is often assumed. The total heat flux by conduction $\dot{Q}_{ci}$ is given by

$$\dot{Q}_{ci} = 4\pi k r_i (T_i - T_\infty). \tag{5}$$

The radius r_i is defined as

$$\frac{r_i}{r_d} = 1 + 2\beta Kn, \tag{6}$$

where β is an experimental coefficient with a best fit value of $\beta = 0.75$ [7]. The Knudsen number Kn is given by

$$Kn = \frac{\lambda}{2r_d}, \tag{7}$$

where λ is the mean free path of the molecules. This is often defined as the distance between two collisions of

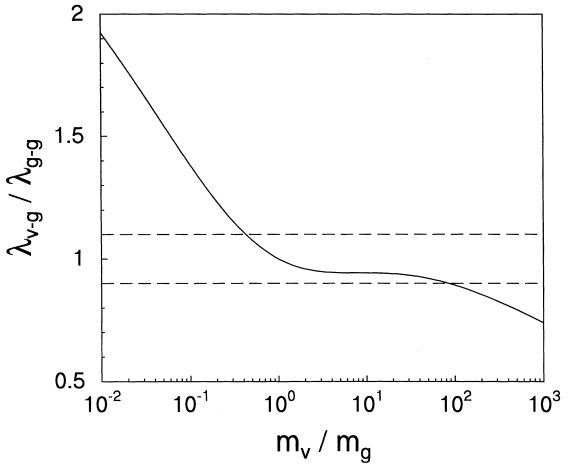

Fig. 4. Ratio of the mean free path of a vapour molecule in a gas environment to that of a gas molecule in its own environment, as a function of their mass ratio.

a molecule. However, a better definition is to take it as the average step size of a random walk, i.e. the average length over which a molecule "loses its sense of direction". From elementary gas kinetics [17] it can be shown that

$$\lambda = \frac{2}{n_{\mathrm{tar}}\pi(d_{\mathrm{col}} + d_{\mathrm{tar}})^2\sqrt{\frac{m_{\mathrm{tar}}}{m_{\mathrm{col}}+m_{\mathrm{tar}}}}}, \tag{8}$$

where n_{tar} is the number density of target molecules, while m and d denote the mass and collision diameter of a molecule. Obviously, λ depends on the masses of the interacting molecules. Since we are considering dilute vapours, the dominant interaction for the mass transport is vapour–gas collision. On the other hand, for the energy transport the gas–gas interaction is dominant. So, in principle, two different mean free paths play a role. It is therefore useful to investigate how the ratio of the masses of the interacting molecules influences the ratio of the different mean free paths. This is shown in Fig. 4. Apparently, the ratio of the mean free paths varies between 0.9 and 1.1 as long as the ratio $(m_{\mathrm{v}}/m_{\mathrm{g}})$ lies between 0.43 and 86 (assuming $d \sim m^{1/3}$). Hence, it is reasonable to use only one mean free path for the cases considered here. This will be the expression for the gas–gas interaction, being

$$\lambda = \frac{1}{n_{\mathrm{g}} d_{\mathrm{g}}^2 \pi\sqrt{2}}. \tag{9}$$

The collision diameter d_{g} is taken to be the Lennard–Jones diameter of the carrier gas, determined from viscosity data [18]. The number density n_{g} is straightforwardly determined from the gas density.

Now we have two expressions as well for the mass as for the energy flux (Eqs. (1)–(4)). To calculate the variables $\dot{M}$, $\dot{E}$, ρ_{vi}, ρ_{gi}, T_{d} and T_{i}, two additional equations are required. One of these is obtained by the droplet energy equation. Since all the energy is produced on account of the condensing vapour, one can write

$$\dot{E} = \frac{\mathrm{d}}{\mathrm{d}t}(M_{\mathrm{d}}h_{\mathrm{d}}) = \dot{M}h_{\mathrm{d}} + M_{\mathrm{d}}\dot{h}_{\mathrm{d}}, \tag{10}$$

where M_{d} and h_{d} are the total mass and the specific enthalpy of the droplet, respectively. Since we are considering steady-state growth, the second term on the right hand side of Eq. (10) is negligible. The remaining equation can be rewritten as

$$\dot{E} = -\dot{M}(h_{\mathrm{vs}} - h_{\mathrm{d}}) + \dot{M}h_{\mathrm{vs}} = -\dot{M}L + \dot{M}h_{\mathrm{vs}}, \tag{11}$$

where L is the latent heat of condensation. The sixth equation, to make the system complete, is the equation of state:

$$\rho_{\mathrm{gi}} + \rho_{\mathrm{vi}} = \frac{p}{ZRT_{\mathrm{i}}}. \tag{12}$$

Here $Z \approx Z_{\mathrm{g}}$ and is calculated from p and T_∞ using an equation of state proposed by Sychev et al. [19,20].

Note that in the original work by Young [7] all the equations were written in terms of partial pressures. Here we have rewritten them in terms of partial densities, enabling us to take into account real gas effects.

3.2. The Gyarmathy model

Gyarmathy extensively describes [6] droplet growth, including the relative flow between the droplet and the gas mixture. As mentioned before, we will only consider droplet growth in a quiescent environment. Gyarmathy starts by comparing models based on the flux matching method to experimental results, and then suggests certain modifications. These modifications result in mass and energy fluxes that are reduced to an interpolating fit between the free molecular limit and the continuum limit, and can be written as [10]

$$\dot{M} = \frac{\dot{M}^{\mathrm{ct}}\dot{M}^{\mathrm{fm}}}{\dot{M}^{\mathrm{ct}} + \dot{M}^{\mathrm{fm}}} \tag{13}$$

and,

$$\dot{E} = \frac{\dot{E}^{\mathrm{ct}}\dot{E}^{\mathrm{fm}}}{\dot{E}^{\mathrm{ct}} + \dot{E}^{\mathrm{fm}}}. \tag{14}$$

The fluxes in the free molecular and continuum regime are calculated in a similar manner as is done in the Young model. The equations for the mass and energy fluxes in the continuum regime are

$$\dot{M}^{\mathrm{ct}} = 4\pi r_{\mathrm{d}}\rho_{\mathrm{m}}D_{\mathrm{m}}(y_{\mathrm{vs}} - y_{\mathrm{v}\infty}), \tag{15}$$

and

$$\dot{E}^{\mathrm{ct}} = \frac{1}{2}\dot{M}^{\mathrm{ct}}c_{\mathrm{pv}}(T_{\mathrm{d}} + T_\infty) + 4\pi r_{\mathrm{d}}k_{\mathrm{m}}(T_{\mathrm{d}} - T_\infty). \tag{16}$$

The equations describing the mass and energy fluxes in the free molecular regime are

$$\dot{M}^{\mathrm{fm}} = 4\pi r_{\mathrm{d}}^2\left(\frac{\alpha_{\mathrm{ev}}\rho_{\mathrm{vs}}R_{\mathrm{v}}T_{\mathrm{d}}}{\sqrt{2\pi R_{\mathrm{v}}T_{\mathrm{d}}}} - \frac{\alpha_{\mathrm{con}}\rho_{\mathrm{v}\infty}R_{\mathrm{v}}T_\infty}{\sqrt{2\pi R_{\mathrm{v}}T_\infty}}\right), \tag{17}$$

$$\dot{E}^{\mathrm{fm}} = 4\pi r_{\mathrm{d}}^2 \left[\frac{\rho_{\mathrm{v}\infty} R_{\mathrm{v}} T_\infty \left(c_{\mathrm{pv}} - \frac{R_{\mathrm{v}}}{2} \right)}{\sqrt{2\pi R_{\mathrm{v}} T_\infty}} + \frac{\rho_{\mathrm{g}\infty} R_{\mathrm{g}} T_\infty \left(c_{\mathrm{pg}} - \frac{R_{\mathrm{g}}}{2} \right)}{\sqrt{2\pi R_{\mathrm{g}} T_\infty}} \right] (T_{\mathrm{d}} - T_{\mathrm{i}}) + \dot{M}^{\mathrm{fm}} \left(c_{\mathrm{pv}} - \frac{R_{\mathrm{v}}}{2} \right) T_{\mathrm{d}}. \tag{18}$$

Eq. (17) is of course equal to the familiar Hertz–Knudsen relation. We have thus obtained six equations for the seven unknowns $\dot{M}$, $\dot{M}^{\mathrm{ct}}$, $\dot{M}^{\mathrm{fm}}$, $\dot{E}$, $\dot{E}^{\mathrm{ct}}$, $\dot{E}^{\mathrm{fm}}$ and T_{d}. Eq. (11), relating the energy flux to the mass flux, completes the description.

3.3. Stepwise growth calculations

As input variables to the growth models, we need the temperature T_∞ and the densities ρ_{vs}, $\rho_{\mathrm{v}\infty}$ and $\rho_{\mathrm{g}\infty}$. Since these are not directly measured in the experiments, they have to be calculated from other (measured) quantities.

The far field temperature T_∞ is obtained from the dynamic pressure signal $p(t)$ using the equation of state proposed by Sychev et al. [19,20]. These temperature calculations also provide the compressibility Z_∞ of the gas at far field conditions. Since the total pressure is uniform and the temperature difference $T_{\mathrm{d}} - T_\infty$ is generally small, the compressibility is assumed to be uniform and equal to Z_∞ throughout the gas phase.

Prior to the actual experiment, the initial molar vapour fraction $y_{\mathrm{v}0}^{\mathrm{m}}$ is measured. Due to vapour depletion, this fraction diminishes during droplet growth according to:

$$y_{\mathrm{v}\infty}^{\mathrm{m}}(t) = y_{\mathrm{v}0}^{\mathrm{m}} - \frac{Z_{\infty 0} R_{\mathrm{v}} T_{\infty 0}}{p_0} \times n_{\mathrm{d}0} \frac{4}{3} \pi \rho_{\mathrm{l}} r_{\mathrm{d}}^3(t), \tag{19}$$

where $n_{\mathrm{d}0}$ is the initial number density of droplets, which depends on the nucleation pulse conditions p_0 and $T_{\infty 0}$. Accordingly, the far field (mass) densities are obtained from

$$\rho_{\mathrm{v}\infty} = y_{\mathrm{v}\infty}^{\mathrm{m}}(t) \frac{p}{Z_\infty R_{\mathrm{v}} T_\infty}, \tag{20}$$

$$\rho_{\mathrm{g}\infty} = \left[1 - y_{\mathrm{v}\infty}^{\mathrm{m}}(t) \right] \frac{p}{Z_\infty R_{\mathrm{g}} T_\infty}. \tag{21}$$

The vapour density at the droplet surface is equal to its (curvature corrected) saturated value,

$$\rho_{\mathrm{vs}} = \frac{f_{\mathrm{e}} p_{\mathrm{v}}^{\mathrm{s}}}{Z_\infty R_{\mathrm{v}} T_{\mathrm{d}}} \exp\left(\frac{2\sigma}{\rho_l R_{\mathrm{v}} T_{\mathrm{d}} r_{\mathrm{d}}} \right). \tag{22}$$

Here $p_{\mathrm{v}}^{\mathrm{s}}$ is the saturated pressure of the pure vapour and $f_{\mathrm{e}}(p, T)$ is the enhancement factor, accounting for enhanced vapour pressures at elevated total pressures [10,21] ($f_{\mathrm{e,\,N_2}}$(250 K, 50 bar) = 1.27), and σ is the surface tension.

As a starting point for a growth calculation, the initial radius of the droplets has to be known. According to Muitjens [22], nucleated clusters can be assumed stable — i.e. their finite probability of re-evaporation has become negligible — if they contain at least twice the number of molecules of the critical cluster. Using classical nucleation theory [10,12] the following relation is obtained

$$r_{\mathrm{d}0} = 2^{1/3} \frac{2\sigma}{\rho_{\mathrm{l}} R_{\mathrm{v}} T \ln S}, \tag{23}$$

where S denotes the supersaturation of the gas–vapour mixture, which is defined as

$$S = \frac{y_{\mathrm{v}}^{\mathrm{m}} p}{f_{\mathrm{e}} p_{\mathrm{v}}^{\mathrm{s}}}. \tag{24}$$

For the derivation see Refs. [10,21].

The enhancement factor f_{e}, saturated vapour pressure $p_{\mathrm{v}}^{\mathrm{s}}$, surface tension σ, liquid density ρ_{l} and latent heat L are evaluated at the droplet temperature T_{d}. All other physical properties involved are computed at an intermediate temperature T_{m}. According to Hubbard et al. [23], a one-third rule is appropriate:

$$T_{\mathrm{m}} = \frac{1}{3}(2T_{\mathrm{d}} + T_\infty). \tag{25}$$

Using the relations established above, all input variables for the growth models can be recalculated each time step. The remaining unknowns are then iteratively solved from the system of equations for both models. Finally, the droplet radius is updated each time step using conservation of mass:

$$\frac{\mathrm{d}r_{\mathrm{d}}}{\mathrm{d}t} = -\frac{\dot{M}}{4\pi\rho_l r_{\mathrm{d}}^2}. \tag{26}$$

The program calculating the growth patterns is written for the FORTRAN compiler, using several NAG routines.

4. Results and discussion

First, the growth models will be compared with experimental droplet growth curves of the *n*-pentanol–helium system, which stretch from the transition to the continuum regime. Then, the models will be compared with new experimental results considering droplet growth of water in helium and nitrogen, respectively, performed at pressures ranging from 10 to 50 bar.

Consequently, these growth curves are situated in the near continuum regime, and hence, can be used to determine the diffusion coefficients of water in helium and water in nitrogen. Since the value of ρD should be independent of pressure, this will provide an independent check of the validity of the growth models.

4.1. n-Pentanol–helium

As part of an international collaboration, nucleation experiments of *n*-pentanol in helium were performed at Eindhoven University of Technology [8]. Since droplet growth curves are used as a tool to determine nucleation rates, these experiments are now used as a reference system to check the accuracy of the growth models. The nucleation experiments were performed at pressures of approximately 1 bar, resulting in experimental droplet growth curves that start in the transition regime ($0.01 < Kn < 1$).

In Fig. 5 droplet growth curves of *n*-pentanol in helium are shown at four different temperatures. The temperatures indicated are averaged over the low pressure plateau. The error bars of the experimental data fall within the size of the markers. The discontinuities in the growth curves after about 15 ms are caused by the arrival of the shock wave reflected from the low pressure section end wall. This causes a positive jump in pressure and temperature, and consequently the droplets start to evaporate instantaneously. The experiment at the temperature of 260 K shows a decrease of the growth rate at the end of the growth curve, caused by depletion of the vapour. Both models are compared with 42 experiments in total. For the lower temperatures ($248\ \mathrm{K} < T < 256\ \mathrm{K}$) the Gyarmathy model shows best agreement with the experimental results while the Young model predicts too large growth rates. For the higher temperatures ($260\ \mathrm{K} < T < 264\ \mathrm{K}$) the experimental growth curves seem to shift towards the Young model. In Fig. 6 two different graphs are combined in one diagram. First, the predicted mass fluxes, scaled with their free molecular flow values M^{fm}, are plotted as a function of *Kn*. Clearly, the Gyarmathy model predicts a much wider transition regime than the Young model, resulting in mass fluxes that are smaller in the transition regime. This can now be used to help explain the different agreement of the model predictions at different temperatures. Therefore, the experiments shown in Fig. 5 are also plotted in Fig. 6, but now as "trajectories" $Kn(t)$ (right axis). As can be seen, each temperature corresponds to a different range of *Kn*, attaining smaller *Kn* values at higher temperatures. Looking at the "trajectories" $Kn(t)$, it can be concluded that the change from free molecular to transition regime starts at too high *Kn* values for the Young model, and the Gyarmathy model predicts this transition more accurately. On the other hand, the change from the transition to the continuum regime is better described by the Young model, where the Gyarmathy model underestimates the mass fluxes.

4.2. Water–helium and water–nitrogen

The droplet growth experiments of water in helium or nitrogen are performed at high pressures ($10\ \mathrm{bar} < p < 50\ \mathrm{bar}$) and low temperature ($T = 247\ \mathrm{K}$). The experimentally obtained radius squared is plotted as a function of time. The radii squared as they follow from the model predictions of Young and Gyarmathy are also plotted as functions of time. In these models

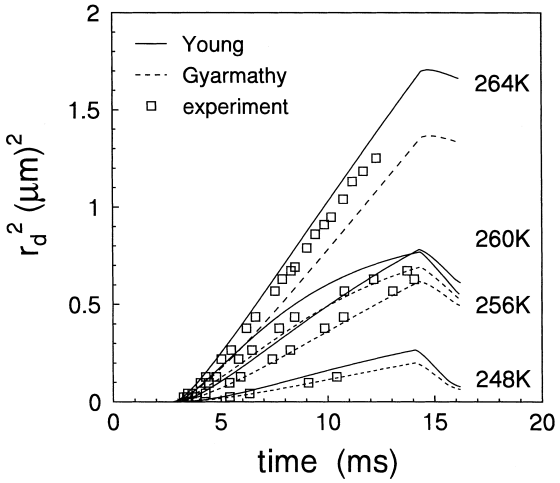

Fig. 5. Droplet growth curves of *n*-pentanol in helium, at pressures near 1 bar.

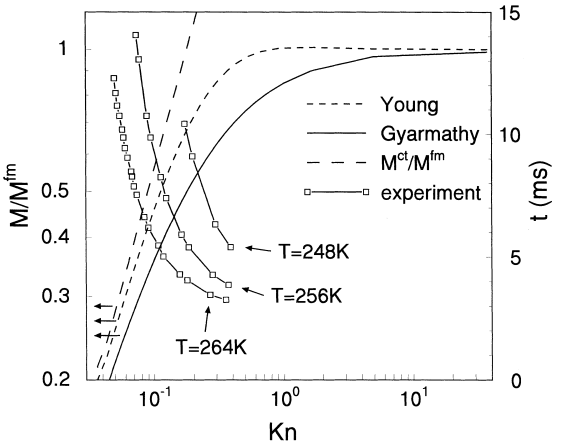

Fig. 6. *n*-pentanol in helium, at pressures near 1 bar. Left axis: scaled mass flux as a function of *Kn* (model). Right axis: time evolution of *Kn* (experiment).

the Fuller correlation [18] is used as an Ansatz value for the diffusion coefficient. In this way, small variations in the growth curve that originate from small variations in the pressure and temperature, are accounted for. Then, the theoretical growth curves are fitted to the experimental results using the diffusion coefficient as a fit parameter. The fit is always performed in a region where the vapour depletion is still negligible, in order to minimize the uncertainty in the value of the diffusion coefficient. This procedure is repeated at each pressure and temperature for a number of experiments.

In Fig. 7 experimental and theoretical growth curves of the water–helium system are shown. The theoretical curves are obtained using the Fuller correlation [18] for the diffussion coefficient. The temperature during the growth of the droplets is approximately 247 K. The average pressures are 11, 27, and 43 bar. The error bars of the experimental data fall within the size of the markers, unless indicated otherwise. The larger errors are caused by the broadening of the Mie peaks due to the slower growth of the droplets. Hence, especially when there is some additional noise in the scattered intensity, the position of the extremum is less precise. In Fig. 8 the fitted diffusion coefficients for the water–helium system are plotted. The product of the specific density ρ_m and the diffusion coefficient D_m should be independent of the pressure. This holds well for the results obtained with the Young model. However, the fitted values obtained using the Gyarmathy model decrease significantly as the pressure increases. This can again be explained by looking at the predicted mass fluxes for the different ranges of *Kn* values covered at each pressure. This is shown in Fig. 9. Note that the mass fluxes are now scaled with their continuum flow values. Looking at the 11 bar experiment in the right plot of Fig. 9 it can be seen that for this

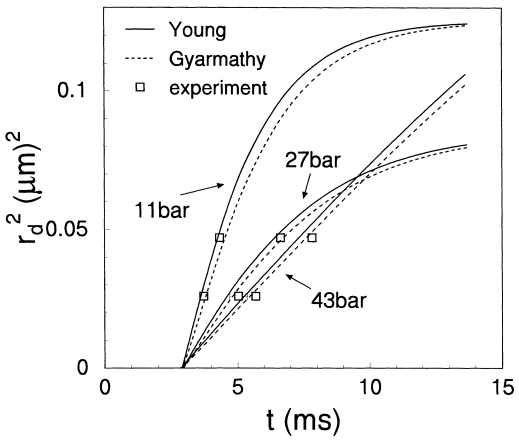

Fig. 7. Droplet growth curves of water in helium ($T \approx 247$ K).

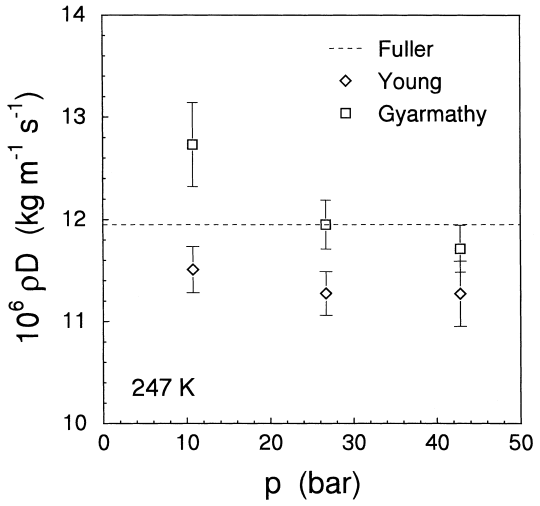

Fig. 8. $\rho_m D_m$ versus p for the water–helium system. The diffusion coefficients D_m are obtained by fitting the Young model and the Gyarmathy model to experimental growth curves.

experiment the *Kn* value is in the range $0.015 < Kn < 0.02$. The Young model predicts (nearly) continuum growth for these values of *Kn*, while according to the Gyarmathy model $0.85 < \dot{M}/\dot{M}^{ct} < 0.9$. Assuming the Young model is correct, the predicted mass flux according to the Gyarmathy model is about 10% too low, corresponding to the about 10% too high value of $\rho_m D_m$ (Fig. 8). As pressure increases *Kn* becomes smaller and the Gyarmathy model also approaches the continuum limit, making the difference between the two models smaller. As a result the diffusion coefficient fitted with the Gyarmathy model approaches the one fitted with the Young model. The transition regime

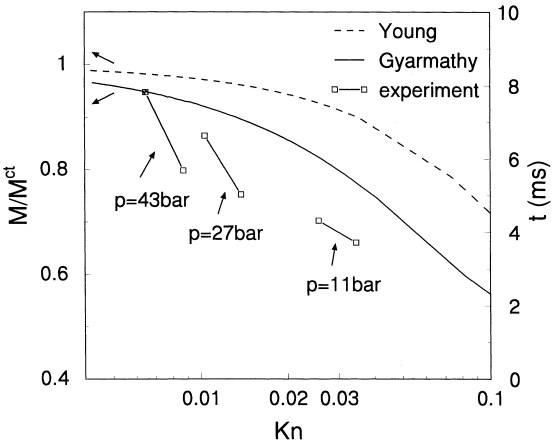

Fig. 9. Water in helium ($T \approx 247$ K). Left axis: scaled mass flux as a function of *Kn* (model). Right axis: time evolution of *Kn* (experiment).

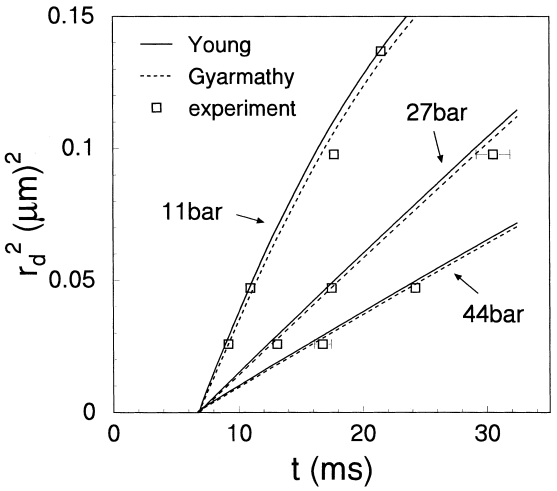

Fig. 10. Droplet growth curves of water in nitrogen ($T \approx 247$ K).

according to the Gyarmathy model stretches too far into the continuum regime. The correct experimental diffusion coefficient is therefore given by the fits with the Young model.

For the water–nitrogen system, generally the same holds as for the water–helium system. Experimental and theoretical (not fitted) growth curves are shown in Fig. 10. Again, the error bars of the experimental data fall within the size of the markers, unless indicated otherwise. The resulting experimentally fitted diffusion coefficients using the two models are shown in Fig. 11. The trends observed are the same as for the water helium system. Looking at the range of Knudsen numbers for each pressure and the matching ratio of $\dot{M}/\dot{M}^{ct}$ (Fig. 12), it can again be concluded that the transition regime according to the Gyarmathy model stretches too far into the continuum regime. Since the 10 bar result of $\rho_m D_m$ fitted with the Young model is a bit higher than the 25 and 40 bar results, one could say that the same holds for the Young model, although less severe. However, the fitted values of $\rho_m D_m$ are independent of pressure, within the experimental error. The experimental diffusion coefficients fitted with the Young model are therefore again considered to be correct.

5. Discussion

From the results stated above, it follows that the quality of both models, depends on the Knudsen range involved. Varying the values of the parameters α_{con}, α_{ev}, and β does not result in an improved performance of the models. The sensitivity of the Young model to the parameter β is shown in Fig. 13. For β values in between 0.75 and 3 the $\dot{M}/\dot{M}^{fm}$ values are only weakly dependent on β. Still, at low Knudsen numbers, a value $\beta = 3$ would yield too high values of $\dot{M}/\dot{M}^{fm}$, which have not been observed.

As mentioned earlier, Peters and Paikert also studied droplet growth using a shock tube. In their paper published in 1989 [12], they compared their experimental results to a model by Gyarmathy, different from the one used here. The model starts from pure continuum growth, and adds a correction term which depends on the size of the mean free path of the molecules. They found good agreement with their experimental results,

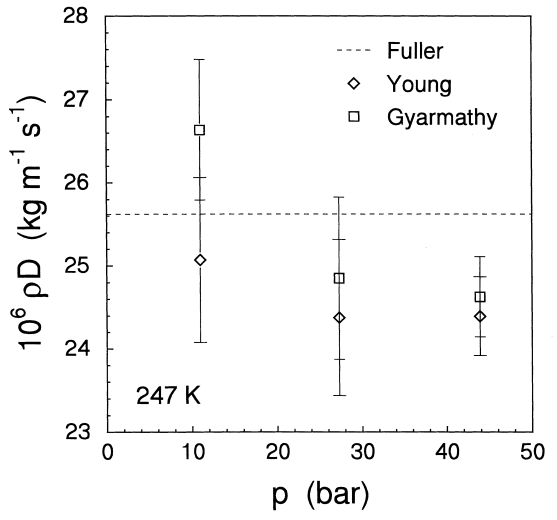

Fig. 11. $\rho_m D_m$ vs. p for the water–nitrogen system. The diffusion coefficients D_m are obtained by fitting the Young model and the Gyarmathy model to experimental growth curves.

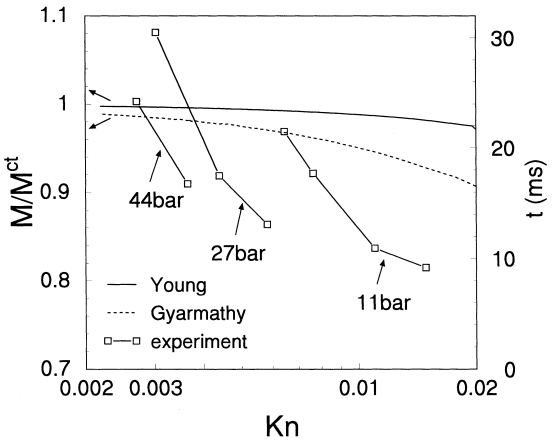

Fig. 12. Water in nitrogen ($T \approx 247$ K). Left axis: scaled mass flux as a function of *Kn* (model). Right axis: time evolution of *Kn* (experiment).

except for very large Knudsen numbers ($Kn > 500$). In their paper of 1994 [13], a different growth model was used to compare their experimental results to. They used the original expressions by Young [7] as a starting point, and modified these by making several approximations. It can be shown that their resulting expressions are very similar to the ones of the Gyarmathy model as it is used here. For the mass flux we obtain the same result if we take the temperature of the droplet and the far field to be equal in our expression. In order to get the same result for the energy flux, the first term on the right-hand side in our Eq. (16) and the last term on the right-hand side of our Eq. (18) have to be neglected. Furthermore, the mean free path as it is defined by Young has to be inserted. Their model predictions and experimental results show excellent agreement for Knudsen numbers down to about $Kn = 0.02$, which is in agreement with our observations. Rodemann and Peters [24] later used the same model, and extended it to include the growth of binary droplets. Again, good agreement was found with experimental results ($Kn < 0.02$), which were now obtained using a piston-expansion-tube.

To evaluate our newly found diffusion coefficient data they are compared with literature data. Therefore, in Figs. 14 and 15 they are shown together with reported data for the water–helium [25,26,28] and water–nitrogen system [25,27], respectively. The reported data are in terms of pressure times diffusion coefficient. This is independent of pressure whenever the ideal gas law is valid and the compressibility Z thus equals one. Our data of density times diffusion coefficient ρD have to be multiplied by the gas constant R and temperature T in order to compare them to the reported results. For the water–helium system the discrepancies with the data previously found in our group by Luijten et al. [25] are quite large. However, the newly found data are regarded as more accurate, for two reasons. First, the determination of the vapour fraction has been improved. But more importantly, the existing data were obtained from fits with the Gyarmathy model, which was then assumed to be correct. Therefore, these data have been reevaluated using the Young model, and the corrected results are also shown in Fig. 14. As can be seen, the data are consistent within the experimental error. For the water–nitrogen system the results are obtained at smaller Kn values, where the difference between the Gyarmathy model and the Young model is very small. Hence, the differ-

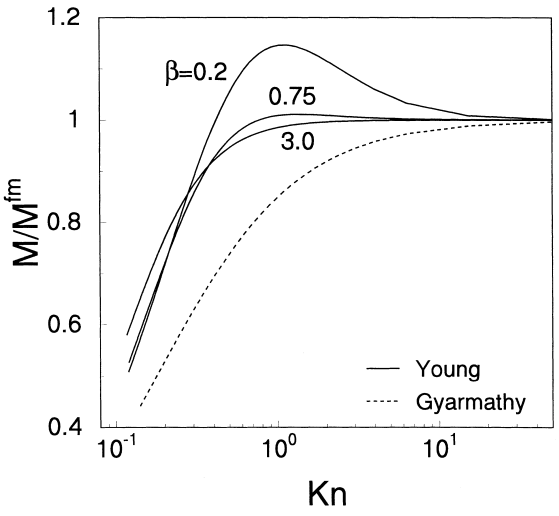

Fig. 13. β-Dependency of the Young model. The Gyarmathy model is also shown in order to get a clear view of the relative changes.

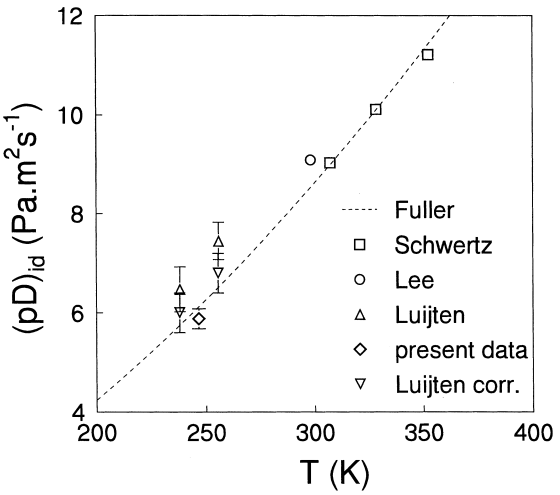

Fig. 14. Diffusion coefficient data of water in helium.

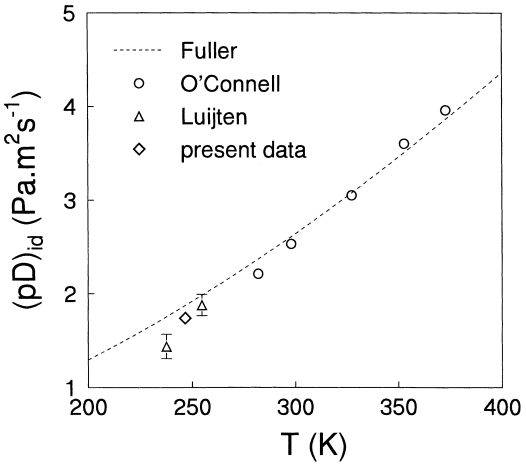

Fig. 15. Diffusion coefficient data of water in nitrogen.

ence in $(pD)_{id}$ when using either the Gyarmathy model or the Young model is negligible and the reported data by Luijten et al. [25] already agree well with our newly found data.

The Fuller correlation, which was used as a reference value for the diffusion coefficient, is also shown in both plots (dotted line). Apparently, this correlation gives diffusion coefficients over a quite large temperature range with error bounds smaller than 5%.

6. Conclusions

The droplet growth models by Gyarmathy and Young have been compared with experimental results. In all cases the model by Gyarmathy predicts a much broader transition regime in terms of the Knudsen number. For the *n*-pentanol–helium experiments this appears to be correct at the upper end of the spectrum (large *Kn*). However, at the lower part of the spectrum (small *Kn*), the Gyarmathy model predicts too low mass fluxes, and the Young model yields more accurate results. This is consistent with the new results obtained from the water–helium and water–nitrogen experiments, which were all located near the continuum regime. An incorrect pressure dependence of the product ρD is found, when the diffusion coefficient is used to fit the Gyarmathy model to the experimental growth curves. This can again be attributed the transition regime stretching too far into the continuum regime, according to the Gyarmathy model. The Young model gives good results for the near continuum regime, and new experimental diffusion coefficient data have thus been obtained. These data are found to be in good agreement with literature data and are well described by the Fuller correlation.

Appendix A. Physical properties

Helium

$M = 4.003$ (kg kmol^{-1}) [18]
$d = 0.2551$ (nm) [18]
$C_p = 5R/2$ (J mol^{-1} K^{-1}) [18]
$k = -2.449 \times 10^{-2} + 1.124 \times 10^{-3}T - 2.929 \times 10^{-6}T^2 + 4.493 \times 10^{-9}T^3 - 2.518 \times 10^{-12}T^4$ (W m^{-1} K^{-1}) [29]

Nitrogen

$M = 28.013$ (kg kmol^{-1}) [18]
$d = 0.3798$ (nm) [18]
$C_p = 31.15 - 1.357 \times 10^{-2}T + 2.680 \times 10^{-5}T^2 - 1.168 \times 10^{-8}T^3$ (J mol^{-1} K^{-1}) [18]
$k^\circ = -6.683 \times 10^{-4} + 1.0558 \times 10^{-4}T - 5.5989 \times 10^{-8}T^2$ (W m^{-1} K^{-1}) [30]
$k = k^\circ(T) + 0.025028 \exp[0.535\frac{pV_c}{ZRT} - 1]$ (W m^{-1} K^{-1}) [18]

n-Pentanol

$M = 88.15$ (kg kmol^{-1}) [18]
$d = 0.6677$ (nm) [18]
$C_p = 3.869 + 0.5045T - 2.639 \times 10^{-4}T^2 + 5.120 \times 10^{-8}T^3$ (J mol^{-1} K^{-1}) [18]
$p^s = 133.324 \exp(90.08 - 9788/T - 9.90 \ln T)$ (Pa) [32]
$\rho_l = \sum_{i=0}^{5} a_i(1 - T/T_c)^{i/3}$,
$a_0 = 270$; $a_1 = 1930.2$; $a_2 = -8414.8$;
$a_3 = 19226.0$; $a_4 = -18559.3$; $a_5 = 6555.7$ (kg m^{-3}) [33]
$L = 67.55 \times 10^3(1 - T/T_c)^{0.8272} \exp(0.8195T/T_c)$ (J mol^{-1}) [34]
$\sigma_0 = 2.6855 \times 10^{-2} - 7.889 \times 10^{-5}(T - 273.15)$ (N m^{-1}) [31]

Water

$M = 18.015$ (kg kmol^{-1}) [18]
$d = 0.2641$ (nm) [18]
$C_p = 32.24 + 1.924 \times 10^{-3}T + 1.055 \times 10^{-5}T^2 - 3.596 \times 10^{-9}T^3$ (J mol^{-1} K^{-1}) [18]
$p^s = 610.8 \exp[-5.1421 \ln(T/273.15) - 6828.77(1/T - 1/273.15)]$ (Pa) [35]
$\rho_l = 999.84 + 0.086(T - 273.15) - 0.0108(T - 273.15)^2$ (kg m^{-3}) [36]
$L = 5.382 \times 10^3[7.08(1 - T/T_c)^{0.354} + 3.767(1 - T/T_c)^{0.456}]$ (J mol^{-1}) [18]
$\sigma_0 = 0.127245 - 1.89845 \times 10^{-4}T$ (fitted for $T <$ 268 K) (N m^{-1}) [37]

A1. Binary diffusion, vapour pressure enhancement and surface tension

For *n*-pentanol–helium the Chapman–Enskog correlation is used [18]. Required values for the Lennard–Jones parameters ϵ and σ were fitted to literature diffusivity data by Ždímal [31], resulting in $\epsilon_{12}/k_B = 55.75$ K and $\sigma_{12} = 0.4614$ nm. After substitution of these values, and eliminating the pressure in favour of the mass density, the remaining relation is

$$\rho D = 2.174 \times 10^{-7}\Omega_D^{-1}(T/\mathrm{K})^{0.5} \left(\mathrm{kg\,m^{-1}\,s^{-1}}\right)$$

The collision integral Ω_D is a function of the dimensionless temperature $\tau = T/\epsilon_{12}$ [18]:

$$\Omega_D = \frac{1.06036}{\tau^{0.15610}} + \frac{0.19300}{\exp(0.47635\tau)} + \frac{1.03587}{\exp(1.52996\tau)} + \frac{1.76474}{\exp(3.89411\tau)}$$

For all helium systems, f_e is evaluated including only

the Poynting-effect:

$$f_e = \exp\left[\frac{M(p - p_{sat})}{\rho_l RT}\right]. \tag{A1}$$

Enhancement factors for water in nitrogen are given by Ref. [10]

$$f_e = \exp\left[b(T) \times (p - p_{sat})\right], \tag{A2}$$

with p in bar and where

$$b(T) = 4.420 \times 10^{-2} - 3.03 \times 10^{-4} T + 7.31 \times 10^{-7} T^2 - 5.98 \times 10^{-10} T^3. \tag{A3}$$

For water–nitrogen, a pressure dependent term is added to the surface tension, resulting in [10]

$$\sigma = \sigma_0 - 6 \times 10^{18} k_B T \ln\left[\frac{p + 326}{326}\right]. \tag{A4}$$

Here, the pressure p should again be taken in bar.

Appendix B. Continuum fluxes

The conservation of mass

$$\frac{d}{dr}\left[r^2 \rho u\right] = 0 \tag{B1}$$

can be rewritten in the form

$$\frac{d}{dr}\left[r^2 \rho_v (u + v_v) + r^2 \rho_g (u + v_g)\right] = 0. \tag{B2}$$

Here the partial densities ($\rho = \rho_v + \rho_g$) and the definition of diffusion fluxes ($\rho_v v_v + \rho_g v_g = 0$) were used. Assuming that the gas does not enter the droplet ($u + v_g = 0$) this can be written as

$$\frac{d}{dr}\left[r^2 \rho_v (u + v_v)\right] = 0. \tag{B3}$$

Assuming steady state, integration of Eqs. (B1) and (B3) give the constant mass flux

$$\dot{M} = 4\pi r^2 \rho u = 4\pi r^2 \rho_v (u + v_v). \tag{B4}$$

Writing the diffusion flux as:

$$\rho_v v_v = -\rho D \frac{d}{dr}\frac{\rho_v}{\rho}, \tag{B5}$$

and combining this with Eq. (B4), the following result can be obtained

$$\dot{M}(1 - y_v) = -4\pi r^2 \rho D \frac{dy_v}{dr}, \tag{B6}$$

where the vapour mass fraction $y_v = \rho_v/\rho$ was introduced. For small vapour mass fractions ($y_v \ll 1$) the term ρD is independent of y_v, and Eq. (B6) can be readily integrated, yielding

$$\dot{M} = 4\pi r_i^2 \rho D \ln\left(\frac{1 - y_{v\infty}}{1 - y_{vi}}\right). \tag{B7}$$

For small vapour mass fractions the logarithmic term can be linearised to give

$$\dot{M} = 4\pi r_i^2 \rho D (y_{vi} - y_{v\infty}). \tag{B8}$$

From the conservation of energy

$$\frac{d}{dr}\left[\rho u\left(h + u^2/2\right) + r^2 \dot{q}\right] = 0, \tag{B9}$$

the (steady state) total energy flux can be obtained by integration:

$$\dot{E} = 4\pi r^2 \rho u\left(h + u^2/2\right) + 4\pi r^2 \dot{q}. \tag{B10}$$

The heat flux per unit area can be written as

$$\dot{q} = -k\frac{dT}{dr} + h_v \rho_v v_v + h_g \rho_g v_g, \tag{B11}$$

where the first term on the right is a conduction term, and the second and third are diffusion terms. Combining Eq. (B10) with Eqs. (B4) and (B11), neglecting the kinetic term, and keeping in mind that $\rho_v v_v + \rho_g v_g = 0$ and $h = (\rho_v/\rho)h_v + (1 - \rho_v/\rho)h_g$, the following result can be obtained

$$\dot{E} = \dot{M} c_{pv} T + 4\pi r^2 k \frac{dT}{dr}, \tag{B12}$$

where $h_v = c_{pv} T$ was used. Integration of this equation yields

$$\frac{\dot{E} - \dot{M} c_{pv} T_i}{\dot{E} - \dot{M} c_{pv} T_\infty} = \exp\left(-\frac{\dot{M} c_{pv}}{4\pi r_i k}\right) = \exp(-\epsilon). \tag{B13}$$

For small ϵ this can be approximated as

$$\frac{\dot{E} - \dot{M} c_{pv} T_i}{\dot{E} - \dot{M} c_{pv} T_\infty} = 1 - \epsilon + \epsilon^2/2, \tag{B14}$$

resulting in

$$\dot{E} = \frac{1}{2}(T_i + T_\infty) c_{pv} \dot{M} + 4\pi r_i k (T_i - T_\infty). \tag{B15}$$

When a first order instead of a second order approximation is made the first term on the right should be replaced by $\dot{M} c_{pv} T_\infty$. For the cases studied in this paper several numerical calculations were carried out both with and without the approximations of the log-

arithm and exponential, and no significant differences were found.

References

[1] J.H. Seinfeld, S.N. Pandis, Atmospheric Chemistry and Physics, Wiley, New York, 1998.
[2] H. Hertz, Ann. Phys 17 (1882) 177.
[3] M. Knudsen, Ann. Phys 47 (1915) 697.
[4] N.A. Fuchs, Ueber die Verdampfungsgeschwindigkeit kleiner Tröpfchen in einer Gasatmosphäre, Phys. Z. Sowjet 6 (1934) 224–243.
[5] N. Fukuta, L.A. Walter, Kinetics of hydrometeor growth from a vaporspherical model, J. Atmos. Sci 27 (1970) 1160–1172.
[6] G. Gyarmathy, The spherical droplet in gaseous carrier streams: review and synthesis, in: Handbook of Chemistry and Physics. Multiphase Science and Technology 1, 62nd ed., McGraw-Hill, New York, 1981-1982, pp. 99–279.
[7] J.B. Young, The condensation and evaporation of liquid droplets at arbitrary Knudsen number in the presence of an inert gas, Int. J. Heat Mass Transfer 36 (1993) 2941–2956.
[8] C.C.M. Luijten, O.D.E. Baas, M.E.H. van Dongen, Homogeneous nucleation rates for *n*-pentanol from expansion wave tube experiments, J. Chem. Phys 106 (1996) 4152–4156.
[9] K.N.H. Looijmans, M.E.H. van Dongen, A pulse expansion wave tube for nucleation studies at high pressures, Exp. Fluids 23 (1997) 54–63.
[10] C.C.M. Luijten. Nucleation and droplet growth at high pressure. Ph.D. thesis, Department of Fluid Dynamics, Eindhoven University of Technology, 1998.
[11] C.C.M. Luijten, P. Peeters, M.E.H. Van Dongen, Nucleation at high pressure. II. Wave tube data and analysis, J. Chem. Phys 111 (1999) 8535–8544.
[12] F. Peters, B. Paikert, Nucleation and growth rates of homogeneously condensing water vapor in argon from shock tube experiments, Exp. Fluids 7 (1989) 521–530.
[13] F. Peters, B. Paikert, Measurement and interpretation of growth and evaporation of monodispersed droplets in a shock tube, Int. J. Heat Mass Transfer 37 (1994) 293–302.
[14] C.C.M. Luijten, L.E. Stormbom, M.E.H. van Dongen, Pressure influence in capacitive humidity measurement, Sens. Act.: B. Chem. 49 (1998) 279–282.
[15] H. Grad, Principles of the kinetic theory of gases, in: S. Flugge (Ed.), Encyclopaedia of Physics, vol. 12, Springer, Berlin, 1958, pp. 205–294.
[16] L. Pong, G.A. Moses, Vapour condensation in the presence of a noncondensable gas, Phys. Fluids 163 (1986) 1796–1804.
[17] M. Mitchner, C.H. Kruger Jr, Partially Ionized Gases, Wiley Series in Plasma Physics, Wiley–Interscience, New York, 1973.
[18] R.C. Reid, J.M. Prausnitz, B.E. Poling, The Properties of Gases and Liquids, McGraw-Hill, New York, 1987.
[19] V.V. Sychev, A.A. Vasserman, A.D. Kozlov, G.A. Spiridonov, V.A. Tsymarny, Thermodynamic Properties of Helium, Springer, Berlin, 1987.
[20] V.V. Sychev, A.A. Vasserman, A.D. Kozlov, G.A. Spiridonov, V.A. Tsymarny, Thermodynamic Properties of Nitrogen, Springer, Berlin, 1987.
[21] C.C.M. Luijten, M.E.H. Van Dongen, Nucleation at high pressure. I. Theoretical considerations, J. Chem. Phys. 111 (1999) 8524–8534.
[22] M.J.E.H. Muitjens. Homogeneous condensation in a vapour/gas mixture at high pressures in an expansion cloud chamber. Ph.D. thesis, Eindhoven University of Technology, 1996.
[23] G.L. Hubbard, V.E. Denny, A.F. Mills, Droplet evaporation: effects of transients and variable properties, Int. J. Heat Mass Transfer 18 (1975) 1003–1008.
[24] T. Rodemann, F. Peters, Measurement and interpretation of growth of binary droplets suspended in a water–*n*-propanol–nitrogen mixture by means of a piston-expansion-tube, Int. J. Heat Mass Transfer 40 (1997) 3407–3417.
[25] C.C.M. Luijten, K.J. Bosschaart, M.E.H. van Dongen, A new method for determining binary diffusion coefficients in dilute condensable vapors, Int. J. Heat Mass Transfer 40 (1997) 3497–3503.
[26] C.Y. Lee, C.R. Wilke, Measurements of vapor diffusion coefficient, Ind. Eng. Chem. 46 (1954) 2381–2387.
[27] J.P. O'Connell, M.D. Gillespie, W.D. Krostek, J.M. Prausnitz, diffusivities of water in nonpolar gases, J. Phys. Chem. 73 (1969) 2000–2004.
[28] F.A. Schwertz, J.E. Brow, Diffusivity of water vapor in some common gases, J. Phys. Chem. 19 (1951) 640–646.
[29] C.-H. Hung, M.J. Krasnopoler, J.L. Katz, Condensation of a supersaturated vapor. VIII. The homogeneous nucleation of *n*-nonane, J. Chem. Phys 90 (1989) 1856–1865.
[30] Least-squares fit to recommended values, in: Y.S. Touloukian, P.E. Liley, S.C. Saxena (Eds.), Thermal Conductivity, Thermophysical Properties of Matter, vol. 3, IFI/Plenum, New York, 1970, p. 69.
[31] Fitted to literature data by V. Ždímal, J. Smolík, collected and distributed within the scope of the International Workshop Group on Nucleation, 1996.
[32] T. Schmeling, R. Strey, Equilibrium vapor pressure measurements for the *n*-alcohols in the temperature range from $-30^{\circ}C$ to $+30^{\circ}C$, Ber. Bunsenges. Phys. Chem. 87 (1983) 871–874.
[33] J.L. Hales, J.H. Ellender, Liquid densities from 293 to 490 K of nine aliphatic alcohols, J. Chem. Thermodyn 8 (1976) 1177–1184.
[34] V. Majer, V. Svoboda, V. Uchytilova, M. Finke, Fluid Phase Equil 20 (1985) 111.
[35] N.B. Vargaftik, Tables on the Thermophysical Properties of Liquids and Gases, 2nd ed., Hemisphere, London, 1975.
[36] H.R. Pruppacher, J.D. Klett, Microphysics of Clouds and Precipitation, Reidel, Dordrecht, 1978.
[37] Least squares fit to data of P.T. Hacker, Experimental values of the surface tension of supercooled water, National Advisory Committee for Aeronautics, 1951, technical note 2510.